

# Hexagonal@Cubic CdS Core@Shell Nanorod Photocatalyst for Highly Active Production of H<sub>2</sub> with Unprecedented Stability

Kui Li, Min Han, Rong Chen, Shun-Li Li, Shuai-Lei Xie, Chengyu Mao, Xianhui Bu, Xue-Li Cao, Long-Zhang Dong, Pingyun Feng,\* and Ya-Qian Lan\*

Using semiconductor-based photocatalytic technology for water splitting to produce H<sub>2</sub> is an ideal way to produce clean solar fuels and remedying environmental problems.<sup>[1]</sup> For this purpose, the key lies in finding proper photocatalysts that can harvest sunlight and efficiently separate photo-generated charge carriers. CdS has a suitable band gap ( $E_g = 2.4$  eV) for visible light absorption and proper conduction band (CB) position for reducing water to produce H<sub>2</sub>,<sup>[2]</sup> making it a potential candidate for photocatalytic water splitting. However, its application is limited by problems such as rapid recombination of charge carriers, as well as low photostability.<sup>[2b,c,3]</sup>

To improve photocatalytic efficiency and stability of CdS, various methods, for example, the integration of CdS with other semiconductors or carbon-based materials, have been studied,<sup>[2b,3a,c]</sup> resulting in the synthesis of a number of CdS-based hetero-nanostructured photocatalysts such as CdS-TiO<sub>2</sub>,<sup>[4]</sup> CdS-ZnS,<sup>[2b]</sup> CdS-MoS<sub>2</sub>,<sup>[2a,3a]</sup> CdS-WS<sub>2</sub>,<sup>[2a]</sup> and CdS-WO<sub>3</sub>.<sup>[5]</sup> Still, photocatalytic activity of these composites for H<sub>2</sub> evolution is low and the stability is far below 100 h. Clearly, new strategies to enhance photocatalytic performance of CdS-based photocatalysts are desirable.

One strategy, fabrication of surface phase junctions by utilizing semiconductor polymorphism, has been shown to be useful in enhancing photocatalytic performance. For example, phase junctions based on rutile-nanoparticle-decorated anatase nanocrystals<sup>[6]</sup> or  $\alpha$ -Ga<sub>2</sub>O<sub>3</sub>-nanodot-patched  $\beta$ -Ga<sub>2</sub>O<sub>3</sub><sup>[7]</sup> were

synthesized and shown to split water into H<sub>2</sub> and O<sub>2</sub> with much enhanced activity over those with single phase structure alone. Similar phenomena were observed in BiVO<sub>4</sub><sup>[8]</sup> and CaTa<sub>2</sub>O<sub>6</sub><sup>[9]</sup> nanoparticle phase junctions. However, significant challenges were encountered when this strategy was applied to CdS. One study found that hexagonal-cubic CdS nanocrystals phase junction actually showed poorer photocatalytic activity than that of pure hexagonal and cubic phase CdS nanocrystals, which was attributed to grain boundaries in the phase junction.<sup>[10]</sup> Hoffmann and co-workers circumvented this issue by inserting Pt between core-shell hexagonal-cubic CdS nanoparticles phase junction, which helped suppress the surface states of hexagonal CdS core and improved the photocatalytic H<sub>2</sub> production rate by a factor of two.<sup>[11]</sup> Still, the challenge remains as to how to fabricate noble metal-free high-quality CdS nanostructure-based phase junction.

Here we report a highly effective low-cost strategy based on the integration of hexagonal-cubic core-shell architecture with nanorod morphology. It takes into consideration advantages of core-shell structures in passivating surface defects of quantum dots,<sup>[1a,b,12]</sup> as well as advantages of 1D nanorods in shortening the electron diffusion length and increasing the light absorption.<sup>[13]</sup> Notably, the formation of hexagonal II-VI nanorod nanocrystals was reported earlier.<sup>[14]</sup>

The synthesis of core-shell type concentric CdS nanorod phase junctions (NRPJs) composed of hexagonal core and cubic shell is based on a facile one-pot hydrothermal method, i.e., direct treatment of cadmium nitrate and thiourea precursor solution at proper temperature with the variable Cd/S precursor molar ratio and reaction time (**Scheme 1**). With the optimized Cd/S precursor molar ratio and reaction temperature, ultrathin cubic shell forms over the hexagonal core. In contrast, pure hexagonal CdS nanorods are generated in sulfur-rich environment. The obtained concentric CdS NRPJs with the ultrathin cubic shell (2.4 nm) show extremely high H<sub>2</sub> production rate with a value of 742.5  $\mu\text{mol h}^{-1}$  (494 times higher than that of pure hexagonal CdS nanorods) and unprecedented photocatalytic stability over 400 h, which is much longer than previously reported metal sulfide-based photocatalysts. Significantly, even under aerobic condition, the CdS NRPJs can continuously operate for over 100 h with H<sub>2</sub> production activity superior to that of pure hexagonal CdS nanorods in vacuum by 108 times.

The CdS NRPJs were fabricated by directly treating Cd(NO<sub>3</sub>)<sub>2</sub> and thiourea precursor solution at 220 °C with properly controlled Cd/S molar ratios and reaction times. The X-ray diffraction (XRD) patterns (**Figure 1a**) indicated that the CdS nanorods made from high content of S precursor (i.e., low Cd/S ratio

Dr. K. Li, Prof. M. Han, Dr. R. Chen, Prof. S.-L. Li, Mr. S.-L. Xie, Dr. X.-L. Cao, Mr. L.-Z. Dong, Prof. Y.-Q. Lan  
Jiangsu Key Laboratory of Biofunctional Materials  
School of Chemistry and Materials Science  
Nanjing Normal University  
Nanjing 210023, China  
E-mail: yqlan@njnu.edu.cn

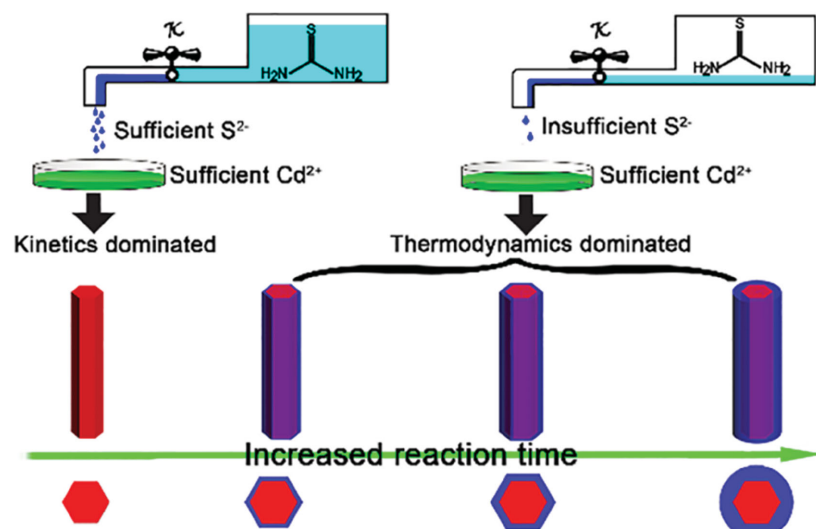
Dr. K. Li  
School of Materials Science and Engineering  
University of Jinan  
Jinan 250022, China

Dr. C. Mao, Prof. P. Feng  
Department of Chemistry  
University of California  
Riverside, CA 92521, USA  
E-mail: pingyun.feng@ucr.edu

Prof. X. Bu  
Department of Chemistry and Biochemistry  
California State University  
Long Beach, CA 90840, USA



DOI: 10.1002/adma.201601047



**Scheme 1.** Schematic illustrating the formation process of concentric CdS NRPs composed of hexagonal core and cubic shell.

at 1:8) showed pure hexagonal phase via kinetics dominated process. As the amount of S supply was reduced, the nucleation rate decreased and the reaction changed from kinetics-dominated to

thermodynamics-dominated process, leading to the formation of hexagonal/cubic CdS phase junction. This trend was more obvious for samples prepared at 180 °C (Figure S1, Supporting Information), where the sample with the lowest S supply leads to the formation of pure cubic phase. Remarkably, CdS phase junction could be obtained in the temperature range from 180 to 240 °C by adjusting the Cd/S ratio (Figure S2, Supporting Information). To probe the formation mechanism of CdS phase junction, NaOH and ethylenediamine (EDA) alkaline solutions were used to facilitate the dissociation of thiourea. In contrast to the distinct hexagonal-cubic CdS phase junction (Cd/S = 1:0.5) in neutral deionized water, the CdS prepared with the same synthetic parameters (i.e., Cd/S ratio and reaction temperature and time) derived from alkaline solutions showed pure hexagonal phase which is attributed to the higher dissociation rate of thiourea

(Figure S3, Supporting Information).

Scanning electron microscopy (SEM) (Figure S4, Supporting Information) indicates that the microstructure of CdS changed

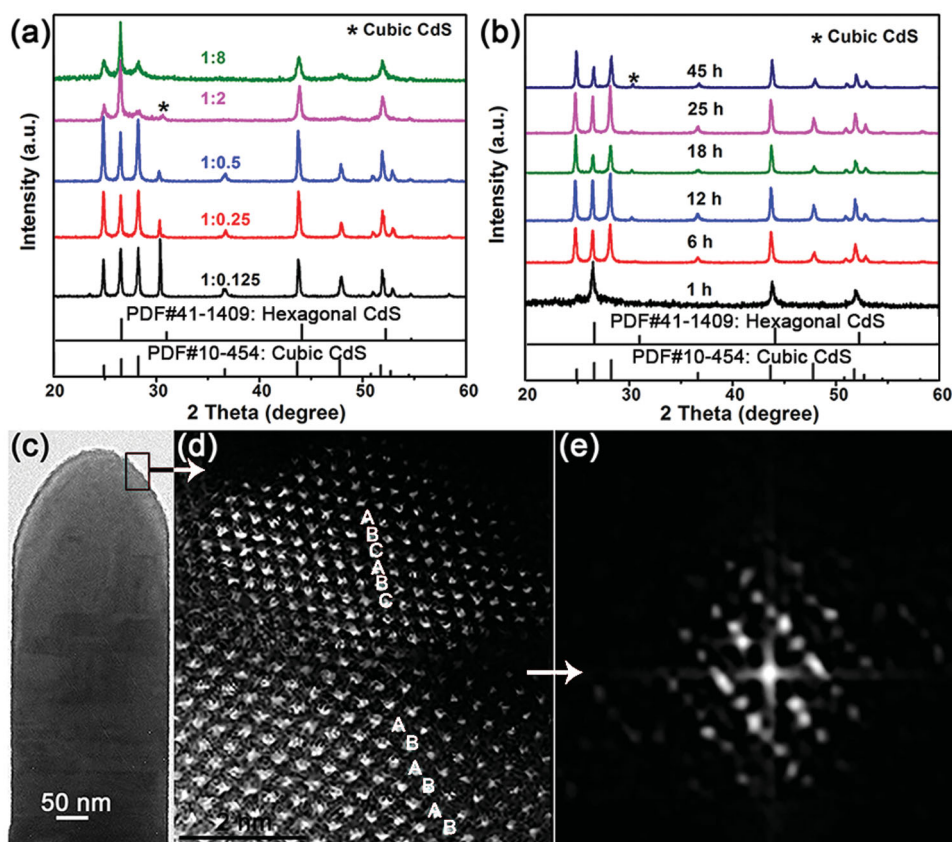


**Figure 1.** XRD patterns of CdS NRPs synthesized at 220 °C under (a) different Cd/S molar ratios and (b) different reaction time, respectively. c) The HRTEM image, (d) HAADF-STEM image, and (e) the corresponding selected area electron diffraction pattern in the interface region of an individual concentric hexagonal-cubic CdS NRP.

from hexagonal prisms to tree-like morphology with increasing S supply. Simultaneously, the increasing thiourea concentration leads to a gradual disappearance of the cubic CdS phase (Figure 1a), and a reduction of the photocatalytic H<sub>2</sub> production rate (Figure S5, Supporting Information). Notably, the sample with pure hexagonal phase (Cd/S = 1/8) shows an extremely low hydrogen evolution rate. The samples prepared at 180 °C behaved similarly (Figure S6, Supporting Information), and the photocatalytic activities of the samples with the optimal ratio of Cd/S at temperatures up to 240 °C were shown in Figure S7 (Supporting Information). These results confirm the extremely important role of CdS phase junction in improving its photocatalytic activity.

To investigate the formation mechanism of hexagonal/cubic CdS phase junction, the CdS samples with the optimal Cd/S ratio (1:0.5) were fabricated with different reaction times at 220 °C and abbreviated as CS $\alpha$  ( $\alpha$  = 1, 6, 12, 18, 25, and 45 h). The Cd<sup>2+</sup> from completely dissolved cadmium nitrate is always sufficient, whereas the continuous reaction decreases the content of thiourea, and causes the insufficient S<sup>2-</sup> (Scheme 1). Consequently, the cubic CdS formed due to the change from kinetics-dominated to thermodynamics-dominated process with the reduced amount of S<sup>2-</sup> in longer reaction time (Figure 1b). A similar trend was found in the samples prepared at 180 °C (Figure S8, Supporting Information). The SEM images (Figure S9, Supporting Information) indicate that CS1 exhibits hexagonal prism morphology, and CS12 and CS18 show similar morphology due to their very limited shell thickness. A further increase in shell thickness causes the disappearance of this morphology.

The high-magnification transmission electron microscopy (TEM) image of an individual CdS NRPJ (CS18) (Figure 1c) shows the nanorod morphology. As depicted in the high-angle annular dark field-scanning transmission electron microscopy (HAADF-STEM) image (Figure 1d), a resolved phase junction could be observed between the shell and core region. And the stacking mode of the CdS lattice changed from the cubic phase (ABCABC) to the hexagonal phase (ABABAB). The electron diffraction pattern recorded on the interface (Figure 1e) shows streaks, indicating the polytype nature of the CdS NRPJ. The high-resolution transmission electron microscopy (HRTEM) was performed to further investigate the concentric CdS NRPJ and the effect of reaction time on the thickness of the cubic CdS shell. As shown in Figure 2a–d (for details, see Figure S10, Supporting Information), the pure hexagonal CdS (CS1) shows well-defined hexagonal CdS lattice. Notably, a cubic shell with a thickness of about 1.4 nm could be observed in CS12. With the reaction time increasing to 18 h, the cubic CdS shell thickness reaches to 2.4 nm. Further increasing the reaction time leads to an increase of the cubic shell thickness to nearly 5 nm. All these observations are consistent with the proposed mechanism of constructing hexagonal/cubic CdS core/shell phase junction via modulating the kinetic and thermodynamic parameters.

A systematic study of the effect of cubic CdS shell thickness on the photocatalytic H<sub>2</sub> production activity (Figure 2e, details in Figure S11, Supporting Information) shows the extremely important role of cubic CdS shell for improving the photocatalytic activity. The pure hexagonal CdS (CS1) shows very low H<sub>2</sub> production rate of 1.5  $\mu\text{mol h}^{-1}$ . Fascinatingly, the formation of

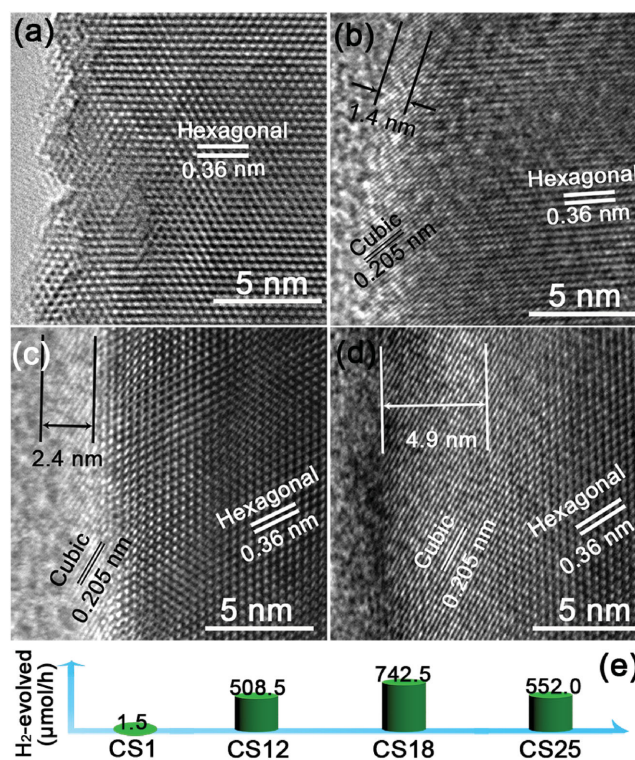


**Figure 2.** a–d) The HRTEM images and (e) photocatalytic H<sub>2</sub> production rate (per 20 mg) of CS1, CS12, CS18, and CS25.

the core/shell phase junction dramatically improved the photocatalytic H<sub>2</sub> production by 252 times even for CS6. The maximal H<sub>2</sub> production rate up to 742.5  $\mu\text{mol h}^{-1}$  with an apparent quantum efficiency (QE) of 43% at 420 nm was obtained for CS18, upon further increasing the reaction time, likely due to the increased crystallinity of cubic CdS shell. This extraordinary H<sub>2</sub> production rate is 494 times higher than that of the pure hexagonal CdS, and compares favorably with the previously reported CdS-based heterostructure (Table S1, Supporting Information).<sup>[2b,e,3a,c,15]</sup> This extremely high photocatalytic activity of CS18 in comparison with the pure hexagonal CdS may come from the passivation of surface trap states of the hexagonal CdS core, and the tunneling of the energetically favorable electrons and holes through the ultrathin cubic CdS shell as reported in CdSe/CdS and CdS/ZnS heterojunctions.<sup>[15f,16]</sup> Moreover, the CS18 exhibited much higher photocatalytic hydrogen production activity than that of cubic CdS (Figure S12, Supporting Information). However, further increasing the shell thickness through longer reaction time leads to a slight reduction of the photocatalytic activity. The effect of reaction time on photocatalytic activity became much more pronounced for the samples prepared at 180 °C (Figure S13, Supporting Information). We have further measured the H<sub>2</sub> evolution of the optimal CdS nanorod phase junctions (CS18) under different wavelength of monochromatic light, and the H<sub>2</sub> evolution plotted against wavelength of monochromatic light is exhibited in Figure S14 (Supporting Information). The hydrogen evolution rate decreased with the increasing wavelength, and the H<sub>2</sub> evolution action spectra coincided with the absorption edge of



the CS18, suggesting the reaction proceeds via photo-absorption by the catalyst. Moreover, the CS18 shows much larger hydrogen production than that of the hexagonal CdS sample at a monochromatic light of 420 nm.

The short lifetime is the most severe drawback of metal sulfide photocatalytic materials. It is highly desirable but challenging to improve their photocatalytic stability. Notably, the optimal CdS NRPJs (CS18) shows an excellent photocatalytic stability over 400 h (Figure 3a), which is much longer than that of hexagonal CdS (only about 10 h) (Figure S15, Supporting Information).<sup>[2b]</sup> The stable junction of the CdS NRPJs was further confirmed by XRD and HRTEM after 400 h reaction (Figure S16, Supporting Information). This extremely long lifetime makes CdS NRPJs the best sulfide photocatalyst owing to the unique CdS core/ultrathin shell phase junction (Table S1, Supporting Information).<sup>[2a,b]</sup> As shown in Figure 3b, different atmospheres were used to further evaluate the photocatalytic activity of CS18. Under N<sub>2</sub> atmosphere, the H<sub>2</sub> evolution rate is lower as the H<sub>2</sub> is not easy to be released. Interestingly, the CdS NRPJs show considerable photocatalytic activity even under aerobic condition, indicating that the as-prepared CdS phase junction may be suitable for practical applications. The lower H<sub>2</sub> evolution rate under aerobic conditions may be ascribed to the inhibition of reaction between photo-generated holes and sacrificial reagent by O<sub>2</sub> and/or the backward reaction of H<sub>2</sub> and O<sub>2</sub> on the photocatalyst surface.<sup>[17]</sup> Notably, this value is still 108 times higher than that of the hexagonal CdS in vacuum. More significantly, the CS18 showed excellent photocatalytic stability even under aerobic condition as confirmed by the stability test over 100 h (Figure 3c).

The X-ray photoelectron spectroscopy (XPS) valence band (VB) spectra indicate that the VB of the hexagonal CdS is 0.13 eV above that of cubic CdS (Figure 4a). Considering the larger bandgap of cubic CdS than its hexagonal counterpart,<sup>[11]</sup> as proved by the UV-vis reflection spectra (Figure 4b), the CB of the cubic CdS is calculated to be upshifted by 0.08 eV and the as-prepared CdS NRPJ shows the type I heterojunction.<sup>[11]</sup> The enhanced photocatalytic activity may come from the passivation of surface trap states on hexagonal CdS, as reported in the CdS-ZnS and CdSe-ZnS core-shell structures.<sup>[11,18]</sup> For the hexagonal CdS nanorods, the photo-generated charge carriers are easily transferred to abundant surface trap states where the electrons or the holes with lower energy are not readily available for photocatalytic reactions.<sup>[15f]</sup> In CdS NRPJs, most surface states of the hexagonal CdS core are passivated via the cubic CdS shell, making the electrons and holes energetically favorable for photocatalytic reactions.<sup>[15f]</sup> Thanks to the ultrathin shell thickness of CdS NRPJs, the confined electrons and holes with high energy in the core would tunnel through the cubic CdS shell to the external surface for reactions.<sup>[2b,18]</sup> Thus, the photo-generated holes could be rapidly consumed by the sacrificial reagent and the recombination probability of

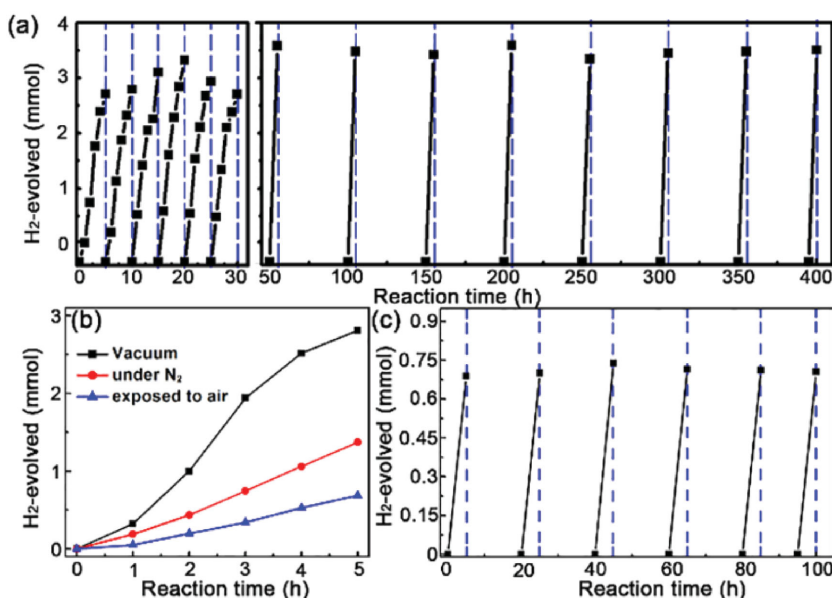


**Figure 3.** a) The photocatalytic stability of CS18 in vacuum under visible light irradiation ( $\geq 420$  nm). b) The photocatalytic H<sub>2</sub> production activity of CS18 under different light conditions. c) The photocatalytic stability of the CS18 under aerobic condition.

electron/hole pairs would be greatly reduced. Further evidence comes from the steady-state photoluminescence (PL) and time-resolved transient-state photoluminescence (TRPL) spectra tests (Figure S16, Supporting Information), which can provide valuable information on the transfer of photo-generated charge carriers and their lifetime. Compared with that of pure hexagonal CdS NRs, the emissions of CdS NRPJs (Figure S17a, Supporting Information) were remarkably quenched and the Stoke's shifts were largely reduced, confirming that the surface trap states of hexagonal CdS cores are effectively passivated and the charge carriers are favorable to penetrate or tunnel across the ultrathin cubic CdS shell. That is to say, the electron-hole recombinations are greatly suppressed in CdS NRPJs, facilitating to boost their photocatalytic performance. Additionally, the TRPL tests (Figure S17b, Supporting Information) reveal that the decay lifetime of charge carriers in CdS NRPJs (0.428 ns) is shorter than that of H-CdS (0.645 ns), implying that the lifetime of photo-generated holes in CdS NRPJs might be very short and rapidly tunneled from the core to the shell surface to be depleted by the sacrificial reagents in solution. While the photo-generated electrons may linger on the catalyst surface and reduce H<sub>2</sub>O to produce H<sub>2</sub>. It should be mentioned that the sample obtained with short reaction time may possess poor crystallization quality of cubic shell and increase the surface defect centers. On the other hand, shells that are too thick will inhibit the tunneling effect of charge carriers.<sup>[2b]</sup> So, CdS NRPJs with proper shell thickness and crystallinity exhibit the highest H<sub>2</sub> production activity.

Furthermore, the transient photocurrents of CS1, CS18, and CS25 showed that the samples (CS18&25) with phase junctions exhibit much higher photocurrents than that of pure hexagonal sample (CS1) (Figure 4c), confirming the importance of cubic CdS shell in the process of charge carriers transfer. Consistent with H<sub>2</sub> evolution tests, the highest photocurrent was

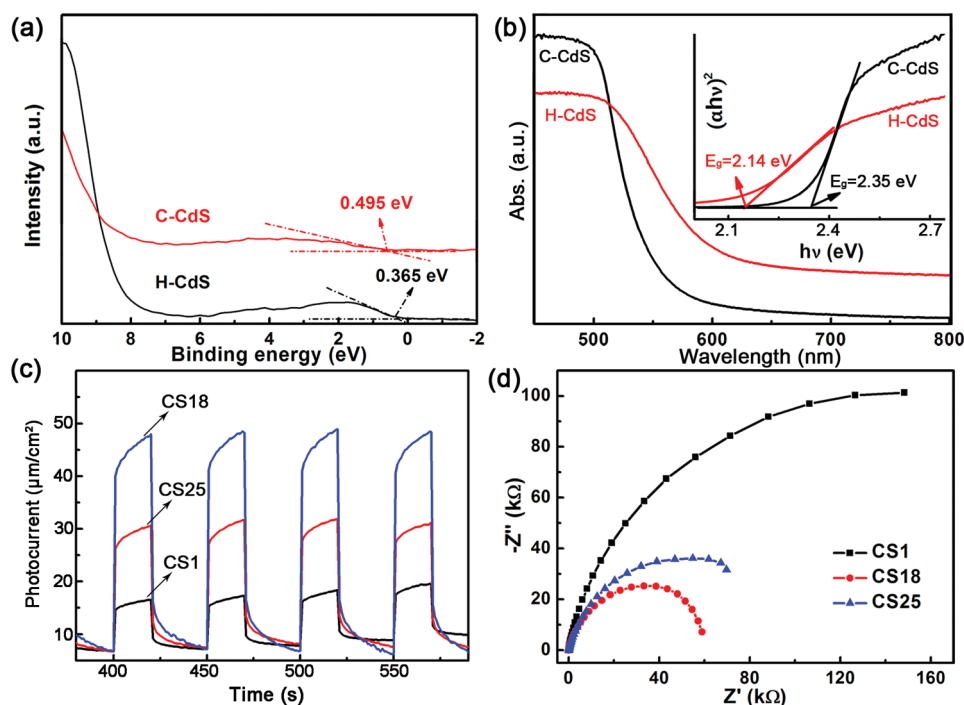


**Figure 4.** a) Valence-band XPS spectra and b) UV–visible diffuse reflection spectra (inset shows the  $(\alpha h\nu)^2$  vs  $h\nu$  curve) for pure cubic and hexagonal CdS samples. c) Transient photocurrent responses and d) Nyquist plots for the samples synthesized at 220 °C under different reaction time.

obtained on CS18, owing to its optimum cubic CdS shell thickness for electron and hole tunneling and superior separation and transfer of charge carriers due to the passivated surface states.<sup>[17,19]</sup> The similar transient photocurrent responses from samples made with the different Cd/S ratios further confirmed the important role of CdS NRPJs in improving photocatalytic activity (Figure S18, Supporting Information). Furthermore, the electrochemical impedance spectra (EIS) analysis (Figure 4d) indicated that CS18 exhibited the smallest semicircle in the middle-frequency region, indicating its fastest interfacial charge transfer due to the well-modulated CdS NRPJs.

In summary, core–shell concentric CdS NRPJs composed of hexagonal core and cubic shell have been successfully synthesized via directly reacting  $\text{Cd}(\text{NO}_3)_2$  and thiourea precursor solution at proper temperature with variable Cd/S molar ratio and reaction time. The concentric hexagonal–cubic CdS NRPJs with the ultrathin cubic shell (2.4 nm) exhibit extremely high photocatalytic  $\text{H}_2$  yield of  $742.5 \mu\text{mol h}^{-1}$  (494 times higher than pure hexagonal CdS nanorods). Especially, such concentric CdS NRPJs also possess excellent photocatalytic stability over 400 h, much longer than previously reported metal sulfide-based photocatalysts. Moreover, even under aerobic conditions, our concentric CdS NRPJs can persistently operate for 100 h with the photocatalytic  $\text{H}_2$  yield superior to that of pure hexagonal CdS nanorods in vacuum by 108 times. The superior photocatalytic performance of such concentric hexagonal–cubic CdS NRPJs is attributed to the following two reasons: (i) the unique core–shell concentric nanorod geometric structure can facilitate charge transfer (tunneling) through the passivation of surface states and the enhanced tunneling of charge carriers; (ii) the presence of ultrathin cubic shell not only passivates the surface state of

hexagonal core but also reduces the recombination of charge carriers via enhanced tunneling. These findings illustrate that the photocatalytic activity and stability of CdS, and possibly other metal sulfide photocatalysts in general, can be greatly improved by elaborate phase junction engineering at nanoscale.

## Supporting Information

Supporting Information is available from the Wiley Online Library or from the author.

## Acknowledgements

K.L., M.H., and R.C. contributed equally to this work. This work was financially supported by NSFC (Nos. 21371099, 21271105, 21471080, and 21541007), the NSF of Jiangsu Province of China (Nos. BK20130043 and BK20141445), the Priority Academic Program Development of Jiangsu Higher Education Institutions, the Foundation of Jiangsu Collaborative Innovation Center of Biomedical Functional Materials, and NSF (DMR-1506661, P.F.).

Received: February 23, 2016

Revised: June 27, 2016

Published online: August 24, 2016

- [1] a) J. Lim, B. G. Jeong, M. Park, J. K. Kim, J. M. Pietryga, Y.-S. Park, V. I. Klimov, C. Lee, D. C. Lee, W. K. Bae, *Adv. Mater.* **2014**, 26, 8034; b) Q. Zhang, I. Lee, J. B. Joo, F. Zaera, Y. D. Yin, *Acc. Chem. Res.* **2013**, 46, 1816; c) G. Xie, K. Zhang, B. Guo, Q. Liu, L. Fang, J. R. Gong, *Adv. Mater.* **2013**, 25, 3820; d) X. Chen, S. Shen, L. Guo,

- S. S. Mao, *Chem. Rev.* **2010**, *110*, 6503; e) Y. Yu, J. Zhang, X. Wu, W. Zhao, B. Zhang, *Angew. Chem. Int. Ed.* **2012**, *51*, 897.
- [2] a) J. Z. Chen, X. J. Wu, L. S. Yin, B. Li, X. Hong, Z. X. Fan, B. Chen, C. Xue, H. Zhang, *Angew. Chem. Int. Ed.* **2015**, *54*, 1210; b) Y. P. Xie, Z. B. Yu, G. Liu, X. L. Ma, H.-M. Cheng, *Energy Environ. Sci.* **2014**, *7*, 1895; c) Q. Li, X. Li, S. Wageh, A. A. Al-Ghamdi, J. Yu, *Adv. Energy Mater.* **2015**, *5*, 1500010; d) K. Chang, Z. W. Mei, T. Wang, Q. Kang, S. X. Ouyang, J. H. Ye, *ACS Nano* **2014**, *8*, 7078; e) Q. Wang, J. Li, Y. Bai, J. Lian, H. Huang, Z. Li, Z. Lei, W. Shangguan, *Green Chem.* **2014**, *16*, 2728.
- [3] a) X. Zong, H. Yan, G. Wu, G. Ma, F. Wen, L. Wang, C. Li, *J. Am. Chem. Soc.* **2008**, *130*, 7176; b) X. Ma, Y. Zhang, Y. Zhang, C. Peng, Y. Che, J. Zhao, *Adv. Mater.* **2015**, *27*, 7746; c) Q. Li, B. Guo, J. Yu, J. Ran, B. Zhang, H. Yan, J. R. Gong, *J. Am. Chem. Soc.* **2011**, *133*, 10878; d) Z. Chen, Y.-J. Xu, *ACS Appl. Mater. Interfaces* **2013**, *5*, 13353.
- [4] H. N. Kim, T. W. Kim, I. Y. Kim, S. J. Hwang, *Adv. Funct. Mater.* **2011**, *21*, 3111.
- [5] L. J. Zhang, S. Li, B. K. Liu, D. J. Wang, T. F. Xie, *ACS Catal.* **2014**, *4*, 3724.
- [6] L. J. Zhang, S. Li, B. K. Liu, D. Wang, T. F. Xie, *ACS Catal.* **2014**, *4*, 3724.
- [7] X. Wang, Q. Xu, M. Li, S. Shen, X. Wang, Y. Wang, Z. Feng, J. Shi, H. Han, C. Li, *Angew. Chem. Int. Ed.* **2012**, *51*, 13089.
- [8] J. Cheng, J. Feng, W. Pan, *ACS Appl. Mater. Interfaces* **2015**, *7*, 9638.
- [9] P. Wang, P. Chen, A. Kostka, R. Marschall, M. Wark, *Chem. Mater.* **2013**, *25*, 4739.
- [10] N. Bao, L. Shen, T. Takata, K. Domen, A. Gupta, K. Yanagisawa, C. A. Grimes, *J. Phys. Chem. C* **2007**, *111*, 17527.
- [11] L. A. Silva, S. Y. Ryu, J. Choi, W. Choi, M. R. Hoffmann, *J. Phys. Chem. C* **2008**, *112*, 12069.
- [12] D. Chen, F. Zhao, H. Qi, M. Rutherford, X. Peng, *Chem. Mater.* **2010**, *22*, 1437.
- [13] S. H. Kang, S. H. Choi, M. S. Kang, J. Y. Kim, H. S. Kim, T. Hyeon, Y. E. Sung, *Adv. Mater.* **2008**, *20*, 54.
- [14] a) Z. A. Peng, X. G. Peng, *J. Am. Chem. Soc.* **2001**, *123*, 1389; b) Z. A. Peng, X. G. Peng, *J. Am. Chem. Soc.* **2001**, *123*, 183.
- [15] a) T. Simon, N. Bouchonville, M. J. Berr, A. Vaneski, A. Adrović, D. Volbers, R. Wyrwich, M. Döblinger, A. S. Susha, A. L. Rogach, F. Jäckel, J. K. Stolarczyk, J. Feldmann, *Nat. Mater.* **2014**, *13*, 1013; b) K. Li, R. Chen, S.-L. Li, M. Han, S.-L. Xie, J.-C. Bao, Z.-H. Dai, Y.-Q. Lan, *Chem. Sci.* **2015**, *6*, 5263; c) J. W. Vickers, H. Lv, J. M. Sumliner, G. Zhu, Z. Luo, D. G. Musaev, Y. V. Geletii, C. L. Hill, *J. Am. Chem. Soc.* **2013**, *135*, 14110; d) M. Liu, F. Li, Z. Sun, L. Ma, L. Xu, Y. Wang, *Chem. Commun.* **2014**, *50*, 11004; e) J. Zhang, Y. Wang, J. Jin, J. Zhang, Z. Lin, F. Huang, J. Yu, *ACS Appl. Mater. Interfaces* **2013**, *5*, 10317; f) L. Huang, X. Wang, J. Yang, G. Liu, J. Han, C. Li, *J. Phys. Chem. C* **2013**, *117*, 11584.
- [16] a) K. Wu, Z. Chen, H. Lv, H. Zhu, C. L. Hill, T. Lian, *J. Am. Chem. Soc.* **2014**, *136*, 7708; b) A. Thibert, F. A. Frame, E. Busby, M. A. Holmes, F. E. Osterloh, D. S. Larsen, *J. Phys. Chem. Lett.* **2011**, *2*, 2688.
- [17] Z. Sun, H. Zheng, J. Li, P. Du, *Energy Environ. Sci.* **2015**, *8*, 2668.
- [18] a) J. Huang, K. L. Mulfort, P. Du, L. X. Chen, *J. Am. Chem. Soc.* **2012**, *134*, 16472; b) Z.-J. Jiang, D. F. Kelley, *J. Phys. Chem. C* **2012**, *116*, 12958.
- [19] J. Zhang, J. Yu, M. Jaroniec, J. R. Gong, *Nano Lett.* **2012**, *12*, 4584.